HEAVY FLAVOUR PHYSICS AT ATLAS

R.W.L. JONES [a]
Department of Physics, Lancaster University, Physics Avenue, Lancaster LA1 4YB, England

Early results on heavy flavours and onia from the ATLAS experiment are presented. The signals for various charms states have been identified. Charmonia have also been isolated, and both the prompt and non-prompt production cross-section determined for the J/ψ; allowing comparisons with various theoretical predictions in a kinematic regime not previously accessed. Exclusive B-meson states have been reconstructed, opening the prospect for an exciting programme of study.

1 The ATLAS Experiment

The ATLAS detector [1] has the familiar concentric cylindrical design common for collider experiments. For the studies in this paper, the most important elements are the Inner Detector, which provides precise tracking information, and the Muon Spectrometer, which provides muon identification and precise momentum measurements. The Inner Detector is composed of silicon pixels, silicon strips and a transition radiation tracker. It sits in a solenoidal magnetic field of 2 T, and provides tracking coverage out to a pseudorapidity, η, of 2.5. The nominal Inner Detector performance gives a relative uncertainty on p_T measurements in the barrel ($|\eta| < 1.5$) of $\sigma/p_T \sim 3.4 \cdot 10^{-4} p_T \oplus 0.015$. The Muon Spectrometer provides coverage out to $|\eta| < 2.7$, and sits in an a toroidal B-field with average strength ~ 0.5 T. It provides a fractional muon momentum uncertainty of 10% up to momenta of ~ 1 TeV.

Muons provide a clean signature and Muon triggers are key to most of the heavy flavour measurements. These provide a clean signature. In the early data taking, they could be run without prescaling and momentum thresholds, but as the luminosity increased the single muon triggers had to be prescaled for p_T below 6 GeV; to compensate, di-muon triggers were introduced.

2 Heavy Flavour Production

2.1 Charmonia and Υ states

Charmonia are of interest for several reasons. Firstly, they provide a standard candle for the commissioning and for studying the detector performance. Secondly, they provide important insight into the production mechanisms at play at these energies, and various theoretical predictions can be tested. Finally, they provide an essential building block to exclusive decay channels such as the $B_s \to J/\psi\phi$ and $B_d \to J/\psi K_s$, which are important for measurements of CP violation and the effects of SUSY and other new physics processes.

[a] On behalf of the ATLAS Collaboration

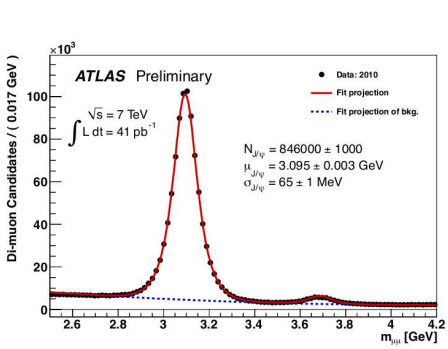

(a) The J/ψ mass region

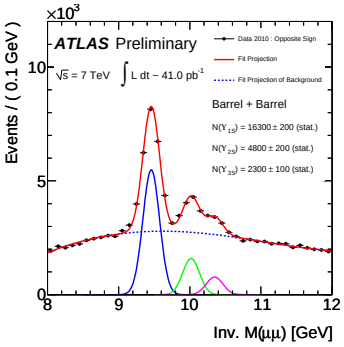

(b) The Υ mass region for candidates with both muons in the barrel of the detector

Figure 1: The charm and bottom onia spectra in dimuon events.

Figure 1 shows the dimuon spectrum using a suite of muon triggers recorded in 41pb^{-1} of 7 TeV data recorded in 2010 [2]. One muon is required to have $p_T > 4$ GeV and the other > 2.5 GeV. The J/ψ and ψ' resonances are clearly evident, with the mass peaks in excellent agreement with the PDG averages. Similar spectra are shown for the Υ mass region in the case where both muons are detected in the barrel region. The $\Upsilon(1S)$ is clearly seem, while the $\Upsilon(2S)$ and $\Upsilon(3S)$ can be distinguished separately. The resolution degrades as one or more of the muons is detected in the barrel end-caps, but a cross-section measurement is possible and underway

2.2 Open charm meson cross-sections

ATLAS has also observed open charm mesons [3,4]. The D_s^+ is reconstructed via the decay chain $D_s^+ \to \phi\pi \to (KK)\pi$, while the D^+ is reconstructed in the decay $D^+ \to K\pi\pi$. The D^{*+} is observed using the usual mass-difference technique, seeking the slow pion peak in the mass difference between D^0 candidates from $K\pi$ combinations and D* candidates from $K\pi\pi$ combinations. In all cases, the fitted mass peaks are in good agreement with PDG averages. These signals have now been used to derive single differential cross-sections for the $D^\pm$ and D^* in p_T and $|\eta|$. These have then been compared with QCD-based Monte Carlo predictions from MC@NLO [5], and from POWHEG [6] applied in PYTHIA [7] and HERWIG [8]. In all cases, the data fall towards the upper range of the predictions, as illustrated for the D^* in Figure 2, and for the $D^\pm$ in Figure 3.

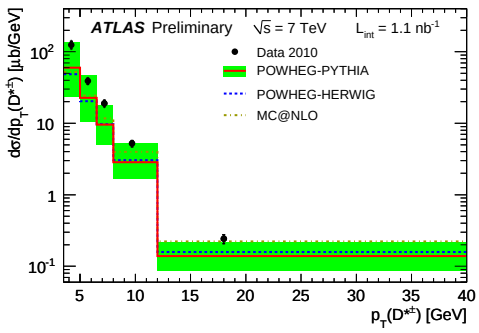

(a) The $D^{*\pm}$ cross-section with respect to p_T.

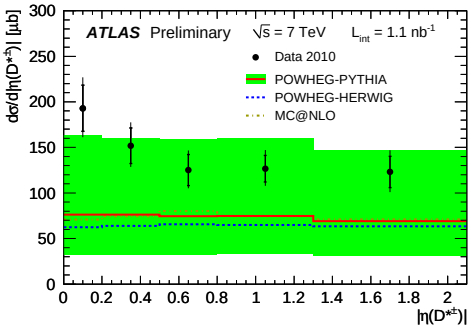

(b) The $D^{*\pm}$ cross-section with respect to $|\eta|$.

Figure 2: The $D^{*\pm}$ production cross-section.

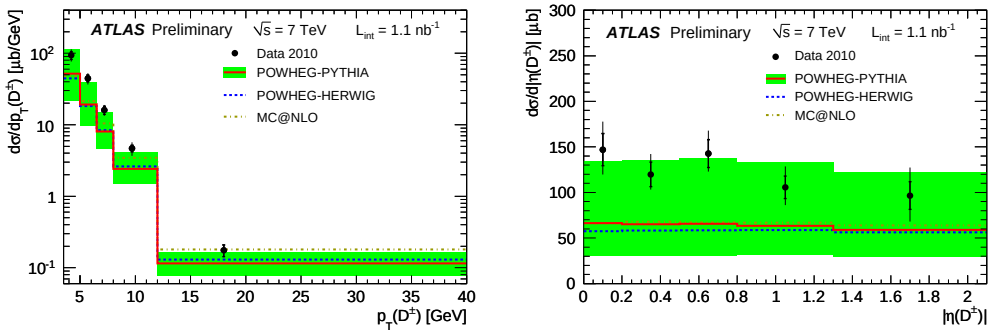

(a) The $D^{\pm}$ cross-section with respect to p_T. (b) The $D^{\pm}$ cross-section with respect to $|\eta|$.

Figure 3: The $D^{\pm}$ production cross-section.

3 The J/ψ differential cross-section

Using the signals identified earlier, ATLAS has derived doubly differential cross-sections for J/ψ production in bins of rapidity, y, and p_T [9]. The measurement requires an extremely well-understood and unbiased trigger selection. As a consequence, low luminosity data is employed and only single muon triggers; at higher luminosities, the pre-scaling would require dimuon triggers to obtain significant statistics, especially at lower p_T, and very many sets with different trigger conditions. The important inputs to the measurement are:

- The acceptance behaviour as a function of the spin-alignment. This is significant, and the true spin-alignment at the LHC is not yet measured. The full range of possibilities is considered in determining the associated systematic uncertainty.
- The muon reconstruction efficiencies. These are determined from the data, using a tag and probe technique.
- The muon trigger efficiencies. These are also obtained from the data; however, there are insufficient statistics to obtain the fine-binning required, so Monte Carlo predictions are used, which are then re-weighted to the measured values in larger bins.

A second measurement is made of the production fraction of non-prompt J/ψ, which are almost entirely produced from B-hadron decays, and often may be distinguished by the finite pseudo decay length. The remainder of the J/ψ are either produced directly or in the feed-down from higher-mass charmonia. The non-prompt fraction is defined as

$$f_B \equiv \frac{d\sigma(pp \to B + X \to J/\psi X')}{d\sigma(pp \to \text{ Inclusive } J/\psi X'')} \tag{1}$$

This observable has the advantage that many systematic effects cancel. This allows combinations of triggers to be employed, leading to increased statistics. For both measurements, the principle of the measurement is simple. The J/ψ yields are extracted from fits to the mass spectra in each p_T and y region. These are then translated into cross-sections by correcting for detector acceptance, reconstruction and trigger efficiencies and for the small effects of bin-to-bin migration. A per-candidate weighting procedure is used, with the weight defined as:

Here, the trigger efficiency is defined as:

$$w^{-1} \quad = \quad \mathcal{A} \cdot \mathcal{M} \cdot \mathcal{E}^2_{\text{trk}} \cdot \mathcal{E}^+{}_{\mu}(p_T^+, \eta^+) \cdot \mathcal{E}^-{}_{\mu}(p_T^-, \eta^-) \cdot \mathcal{E}_{\text{trig}} \tag{2}$$

where $\mathcal{A}$ is the kinematic acceptance, $\mathcal{M}$ is a correction factor for bin migrations due to finite detector resolution, $\mathcal{E}_{\rm trk}$ is the ID tracking efficiency and $\mathcal{E}_{\mu}$ is the single-muon offline reconstruction efficiency. Here $p_T^{\pm}$ and $\eta^{\pm}$ are the transverse momenta and pseudorapidities of the positive and negative muons from the J/ψ decay. The trigger efficiency $\mathcal{E}_{\rm trig}$ for a given J/ψ candidate is calculated from single-muon trigger efficiencies $\mathcal{E}^{\pm}_{\rm trig}(p_T^{\pm}, \eta^{\pm})$ as follows:

$$\mathcal{E}_{\rm trig} = 1 - \left(1 - \mathcal{E}^{+}_{\rm trig}(p_T^{+}, \eta^{+})\right) \cdot \left(1 - \mathcal{E}^{-}_{\rm trig}(p_T^{-}, \eta^{-})\right). \quad (3)$$

The spin-alignment can be characterised by two angles with associated amplitudes, and so the full range of possibilities is limited by the four extreme points and a fifth point where both amplitudes are zero (the flat hypothesis). For the presentation of the results, the flat hypothesis is chosen, with the maximum deviation due to spin-alignment taken as the systematic uncertainty. The inclusive cross-section is shown for two of the four rapidity regions studied in Figure 4 . Also shown are measurements from CMS [10]. As a consequence of the trigger strategies chosen, CMS extend to lower p_T, while ATLAS increases the p_T reach upwards. There is good agreement in the regions of overlap.

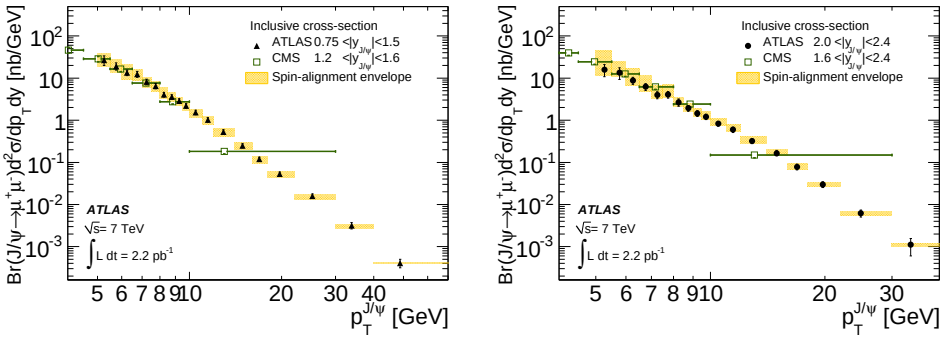

(a) The inclusive $J/'psi$ production cross-section with respect to p_T for one of the lowest of the four $|y|$ bins.

(b) TThe inclusive $J/'psi$ production cross-section with respect to p_T for one of the highest of the four $|y|$ bins.

Figure 4: Illustrative inclusive J/ψ production cross-sections .

The non-prompt fraction determination proceeds in a similar way, but uses the pseudo-proper lifetime and the mass of the candidates in the fits to extract the ratio in bins of p_T and $|y|$. Again, these are compared with CMS [10] and (despite the different centre of mass energy) CDF [11]. There is good agreement between the three experiments, with CDF providing the lowest p_T coverage and ATLAS the high-p_T information, as illustrated in Figure 5 for the lowest of the four rapidity regions studied. Agreement with the CDF point suggests indepdence of the ratio from the center of mass energy.

Combining the two results, the prompt and non-prompt cross-sections can be extracted, as illustrated in Figure 6 for another of the rapidity bins studied. The non-prompt cross-section is compared with the FONLL [12] prediction for $B \to J/\psi X$, and good agreement is found. The prompt cross-section may be compared with various models. Of those used, the previously popular colour evaporation model [13] performs best, but it over-estimates the cross-section at high p_T.

4 Exclusive B-meson decays

In preparation for future studies, various exclusive B-meson decay channels have been investigated. The decay $B^{\pm} \to J/\psi K^{\pm}$ has been reconstructed for both charged states. A clear signal

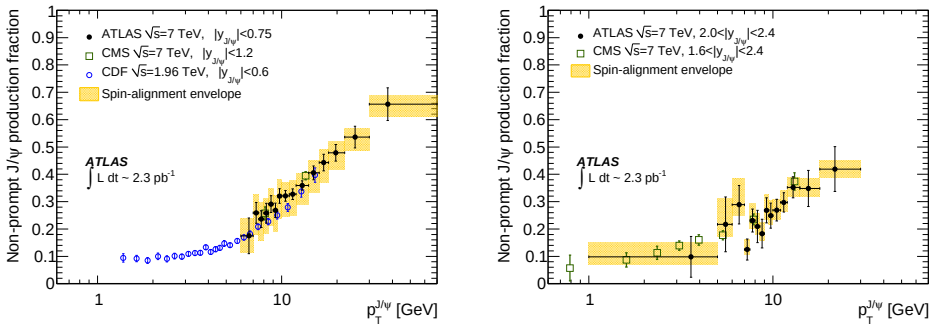

(a) The non-prompt $J/'psi$ production fraction with respect to p_T for the lowest of the four $|y|$ bins studied.

(b) The non-prompt J/ψ production fraction with respect to p_T for the highest of the four $|y|$ bins studied.

Figure 5: Illustrative J/ψ non-prompt production fractions.

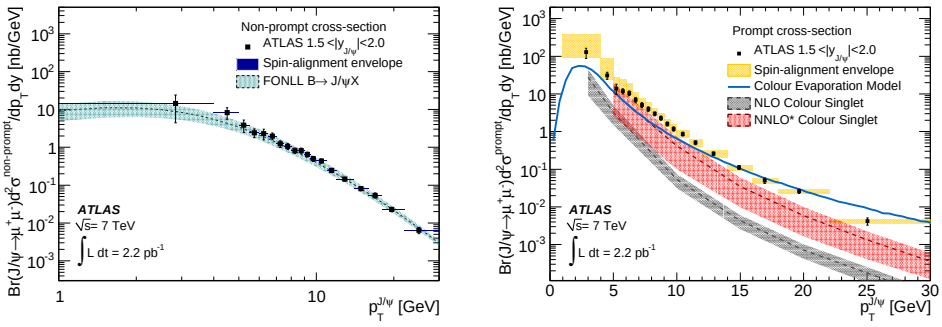

(a) The non-prompt $J/'psi$ production cross-section with respect to p_T for one of the four $|y|$ bins.

(b) The prompt J/ψ production cross-section with respect to p_T for one of the four $|y|$ bins.

Figure 6: Illustrative J/ψ production cross-sections .

is observed even without a cut on the lifetime properties of the candidates (which is important for lifetime-dependent studies), the signal is much purer if one is made, as illustrated in Figure 7. The mass observed is consistent with the PDF value for both selections and for both charged states. Similarly, the decays $B^0 \to J/\psi K^*(K\pi)$ and $B^\pm \to J/\psi\phi(KK)$ have been observed and their masses determined to be consistent with the PDF expectations. Lifetime measurements are underway. These results open the door to lifetime-difference and CP violating weak phase studies as statistics increase.

5 Conclusions

In the first year of 7 TeV data-taking, ATLAS has observed the charm- and bottom-onia states, and has reconstructed important B-meson exclusive decays. Various single-charm states have also been observed and their single-differential production cross-sections measured. Doubly-differential cross-section measurements have been made for the J/ψ, and the prompt fraction determined. Both results extend the previously available kinematic range, agreeing with previous measurements in the areas of overlap. The prompt and non-prompt cross-sections have been extracted and compared with theory. The non-prompt predictions fare well, while the prompt predictions do less well at high p_T. The immediate future includes lifetime measurements, early CP violation studies and as well as studies of the B_c. In the longer term, ATLAS will make

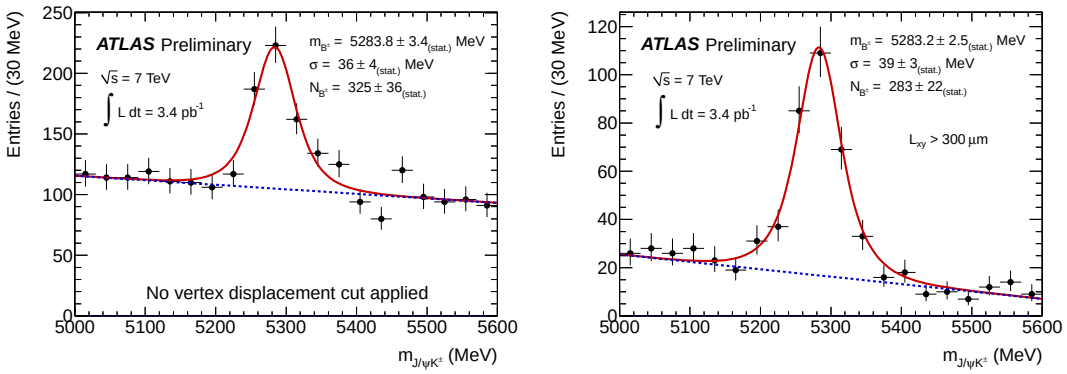

(a) Before lifetime cuts.

(b) After lifetime cuts.

Figure 7: The $B^{\pm}$ signal with and without lifetime cuts.

measurements of rare B-decays to muons.

References

1. ATLAS Collaboration, *JINST* **3**, S08003 (2008)
2. ATLAS Collaboration, ATLAS-CONF-2010-045, http://cdsweb.cern.ch/record/1277685.
3. ATLAS Collaboration, ATLAS-CONF-2010-034 http://cdsweb.cern.ch/record/1277669.
4. ATLAS Collaboration, ATLAS-CONF-2011-017, http://cdsweb.cern.ch/record/1336746.
5. S. Frixione, P. Nason and B. R. Webber, *JHEP* **0308**, 007 (2003) .
6. S. Frixione, P. Nason and G. Ridolfi, *JHEP* **0709**, 126 (2007).
7. T. Sjostrand, S. Mrenna, P. Skands, *JHEP* **05**, 026 (2006).
8. G. Corcella et al., *JHEP* **0101**, 010 (2001).
9. ATLAS Collaboration, G. Aad et al, arXiv:1104.3038 [hep-ex], accepted for publication *Nucl. Phys.* B.
10. CMS Collaboration, arXiv:1011.4193 [hep-ex]
11. CDF Collaboration, D. Acosta et al., *Phys. Rev.* D **71**, 032001 (2005).
12. M. Cacciari, M. Greco and P. Nason, *JHEP* **9805**, 007 (1998)
    M. Cacciari, M. Greco and P. Nason, *JHEP* **0103**, 006 (2001).
13. T. Ullrich, A. D. Frawley and R. Vogt, *Phys. Rep.* **462**, 125 (2008)
    V. D. Barger, W. Y. Keung and R. J. N. Phillips, *Phys. Lett.* B **91**, 253 (1980)
    V. D. Barger, W. Y. Keung and R. J. N. Phillips, *Z. Phys.* C **6**, 169 (2010).
14. ATLAS Collaboration, ATLAS-CONF-2010-098, http://cdsweb.cern.ch/record/1307530.